2018-01-0708

Simplifications Applied to Simulation of Turbulence Induced by a Side View Mirror of a Full-Scale Truck Using DES

Author, co-author (Do NOT enter this information. It will be pulled from participant tab in MyTechZone)
Affiliation (Do NOT enter this information. It will be pulled from participant tab in MyTechZone)

Abstract

In this paper, the turbulent flow induced by a production side-view mirror assembled on a full-scale production truck is simulated using a compressible k-ω SST detached eddy simulation (DES) approach -- the improved delayed DES (IDDES). The truck configuration consists of a compartment and a trailer. Due to the large size and geometric complexity of the configuration, some simplifications are applied to the simulation. A purpose of this work is to investigate whether the simplifications are suitable to obtain the reasonable properties of the flow near the side-view mirror. Another objective is to study the aerodynamic performances of the mirror. The configuration is simplified regarding two treatments. The first treatment is to retain the key exterior components of the truck body while removing the small gaps and structures. Furthermore, the trailer is shaped in an apex-truncated square pyramid. This simplification is proposed based on the assumption that the downstream flow near the trailer has limited effect on the flow near the mirror. To assess the influences of the simplifications, the flow fields computed from the original and simplified configurations are compared. The regions on the window that are subjected to significant hydrodynamic impingement are identified. The mirror and A-pillar introduce the impingement. The frequency spectra of the surface pressure fluctuations on the window are studied. The frequencies of the peaks in the spectra are the same as the characteristic frequencies of the free shear layers that develop from the mirror side-edges near the window. The simplifications are found as feasible treatments to reproduce the flow characteristics of the original geometry.

1. Introduction

To reduce drag and wind noise for modern trucks, considerable efforts have been made in the industry [1]. The aerodynamic performance of a truck can be analyzed and improved by investigating the entire truck body. The approach is too expensive in practice since either experiments or numerical simulations will demand numerous resources to resolve the whole vehicle geometry. An alternative is to study a single component of the body. For example, side-view mirrors [2]. The component is assembled on a flat plate and subjected to a uniform freestream flow. As the complexity and size of the component are reduced as compared to the entire vehicle, the costs of the experimental or numerical resources can be greatly decreased. However, the drawback is that the aerodynamics characteristics of the component assessed using this reduced-order method could be different from those in the real operation conditions, where this component is installed on a vehicle body and interacts with other body components. The presence of a A-pillar could significantly change the characteristics of a side-view mirror, as compared to the case that the side-view mirror is isolated from the vehicle body. The changed characteristics due to the interaction between the mirror and its surrounding environment are described as the installation effect. Besides, the risk of the oversimplification was reported for the interaction between truck fore-body, aft-body and total drag [3].

This study aims to develop a simple numerical benchmark case to investigate the aerodynamics installation effect for a production side-view mirror mounted on a production truck body. The advanced CFD method, detached eddy simulation (DES) [4], will be explored for its suitability in the development of this case. A simplified geometry for the production truck body will be proposed and demonstrated for the purpose of reducing the computational resources that are taken to resolve the geometric details. The feasibility of the simplifications to reproduce the flow field near the A-pillar, the side-view mirror and the window will be assessed. The features of the pressure fluctuations on the window, which could be potentially interesting for the noise generation [2], will be addressed.

The configurations including a production truck and its simplified geometry are presented in the Configurations in Application section. The numerical methodology used in the flow computation is described in the Numerical Methodology section. The numerical settings specified for the computation are provided in the Numerical Settings section. The mesh study is reported in the Computational Meshes section. The results are reported and discussed in the Results and Discussion section. In the Summary section, the findings are summarized.

2. Configurations in Application

The flow simulation is conducted for a full-scale production truck and its simplified geometry. The original and simplified truck geometries are illustrated in Figure 1. The roof bar, which is a bar mounted on the roof to carry horns and lights, has been removed from the original geometry. Furthermore, the simplification includes the following aspects. The small-scale gaps at the connection between the surfaces are sealed. The truck front and the trailer are connected so that the large gap between them is removed. The trailer body is modified to a more streamlined structure. The wheels under the trailer are removed. However, the same mirror, A-pillar and window are mounted on the geometries. These body parts are illustrated in Figure 2. The simplification eliminates resolution of local flow introduced by the geometry components that are far away from the mirror and A-pillar, which account for the flow near the

window. The computational resources for resolving the flow are therefore reduced. Meanwhile, the large-scale influence from the flow guided by the truck front body is retained to take into account the installation effect due to the interaction between the mirror and truck front body.

The freestream velocity vector is $\vec{u}_\infty = (25.16, 0, 0) m/s$ in terms of the coordinate directions illustrated in Figure 3. The freestream pressure is $p_\infty = 101325\ Pa$. The freestream temperature is $T_\infty = 300\ K$. The air is considered as an idea gas with the dynamic viscosity of $1.86 \times 10^{-5} Pa \cdot s$ and the molecular weight of $28.97\ kg/kmol$.

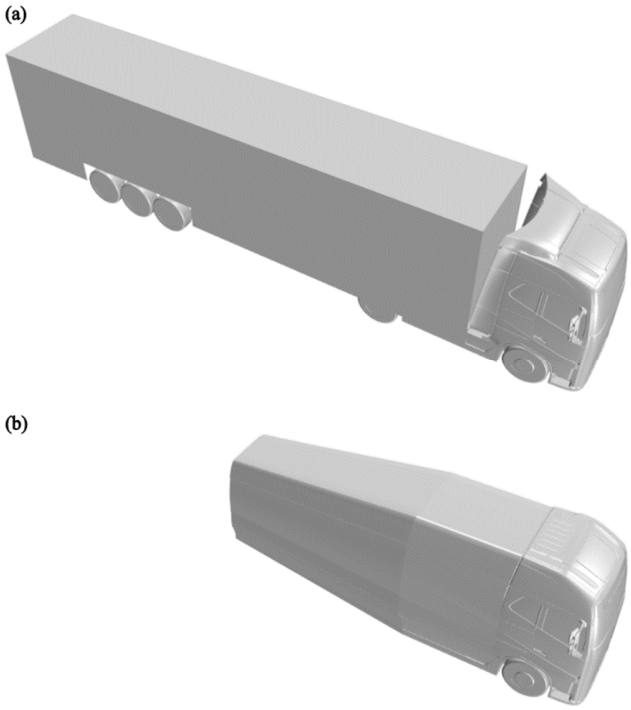

Figure 1. The configurations of the production truck: (a) the original geometry and (b) the simplified geometry.

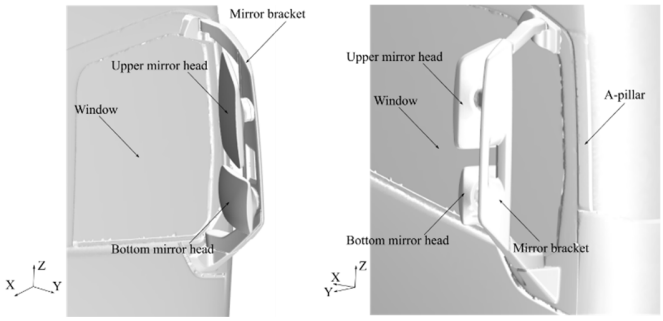

Figure 2. Illustration of the side-view mirror components, the A-pillar and the window.

3. Numerical Methodology

The air is considered as an ideal gas. The flow is compressible. The finite volume method is utilized to discretize the continuity, momentum and energy equations. The simulation in this study is performed using the software STAR-CCM+ [5].

The numerical methodology of the compressible k-ω SST DES introduced hereafter is the same as our study on a generic side-view mirror [6], where compressible and incompressible DES, and compressible LES are used and compared in the simulation of a generic side-view mirror. The methodology is restated as follows.

The segregated flow solver is used to solve the discretized equations. The SIMPLE (Semi-Implicit Method for Pressure-Linked Equations) algorithm is applied to the segregated flow solver. The convection flux on an element face is discretized by means of a hybrid second-order upwind and bounded-central scheme. The diffusion fluxes on the faces of both internal and boundary elements are discretized with a second-order scheme. The second-order hybrid Gauss-LSQ method is used in gradient computation, which involves the reconstruction of the field values on an element face, the secondary gradients of the diffusion fluxes, the pressure gradients and the strain and rotation rates of a turbulence model. A dual time-stepping method with inner iterations at preconditioned pseudo-time steps is used in the time-marching procedure.

The turbulence is simulated using the improved delayed detached eddy simulation (IDDES) [7]. The coefficients of the IDDES model adopt the default values in the software, i.e., $C_{DES,k-\omega} = 0.78$, $C_{DES,k-\varepsilon} = 0.61$, $C_{dt} = 20$, $C_l = 5$ and $C_t = 1.87$. The definitions of the coefficients are the same as those in the user guide [5]. Since the geometries are complex and since velocity over the walls varies in a wide range, it is difficult to ensure that the values of Δy^+ of all elements nearest the walls are either above a high value or below a small value. This problem is solved with the approach of all y^+ wall treatment, which modifies the specific dissipation rate in the near-wall elements [8].

4. Numerical Settings

The computational domain constructed for the simulation is shown in Figure 3. In addition to the simplification of the truck geometry, the symmetry boundary condition is applied to the symmetry plane of the geometry, to simulate half of the geometry instead of the entire one. This treatment reduces the computational costs and memory consumption. The height of the truck front is denoted by H. The value of H is not presented for confidentiality. The length of the configuration is $4H$. The computational domain is a quarter of a cylinder with a radius of $5H$. The distance between the inlet and the configuration is $8H$. The outlet is at a distance of $20H$ from the configuration. The size of the computational domain is chosen in consideration of accommodating the propagation of acoustic waves in the far field so that the magnitudes of the waves at the far-field boundaries are small. The bottom surface of the domain is regarded as the ground. The inflow direction is aligned with the x-axis.

The freestream boundary condition [9] is set at the inlet, the outlet and the side ambient boundary. This boundary condition depresses the acoustic-wave reflection at the boundaries. The non-slip wall boundary condition is set on the geometry surfaces and the ground. The symmetry boundary condition is imposed on the symmetry plane of the truck geometry. It is worth noting that this boundary condition cannot resolve the lateral oscillations in the wake that are caused by the vortex shedding from the truck body. Thus, the integrated wind loads on the truck body cannot be resolved. This is not an issue in the present study since the local flow near the mirror is the focus.

However, this simplification is not generally applicable for numerical investigation of truck aerodynamics using CFD methods.

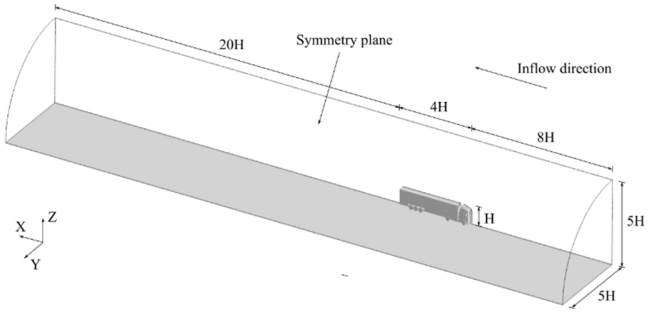

Figure 3. A schematic diagram of the computational domain, which is labeled with dimensions. Here *H* represents the height of the truck front.

The under-relaxation factors for the velocity and the pressure in the segregated flow solver are set to 0.6 and 0.3. The under-relaxation factor for the turbulence transport equations is specified to 0.6.

The time step is set to $\Delta t = 5 \times 10^{-5}\ s$ to achieve the numerical stability in terms of the Courant number. The maximum number of inner iterations at every time step is 20. This number is sufficient to converge the solution according to the preliminary numerical tests performed for the configurations.

5. Computational Meshes

The mesh generation takes a hybrid strategy. Polyhedral elements are generated in the region near the window and mirror. Hexahedral elements of a trimmed mesh [5] are produced in the far field.

The polyhedral mesh generation method can control the growth ratio of element sizes in the near field to a small value so that the numerical errors introduced by the mesh quality in the solution of the acoustic wave propagation are reduced. The growth ratio is set to 1.05 in this study, which is obtained based on previous numerical tests for unstructured meshes [10, 11] and structured meshes [12]. A drawback of this method is that it can in general produce more nodes in a volume than the trimmed mesh generation method. The growth ratio in the latter method is constant and equivalent to 2, which is larger than for the former method.

The partition of the computational domain is shown in Figure 4. The cube enclosing the truck front is treated as the near-field region where the polyhedral mesh generation method is used. The trimmed mesh generation method is employed in the remaining of the domain. The element shapes of the trimmed mesh are illustrated in Figure 5a.

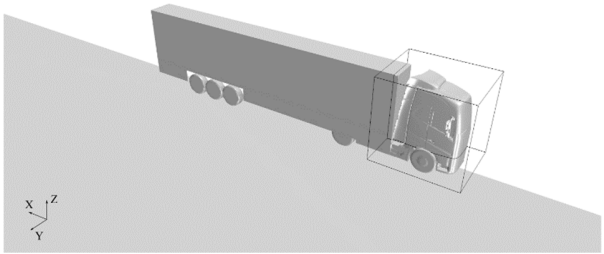

Figure 4. The partition strategy adopted to apply the different mesh generation methods. Here polyhedral elements are generated inside the cube. Trimmed elements are constructed in the rest of the computational domain.

Based on the hybrid generation strategy, the mesh generator of STAR-CCM+ is used to produce the meshes for the original and simplified configurations. The surface elements of the original configuration are shown in Figure 5. The polyhedral element sizes are $5 \times 10^{-3}m$ on the mirror, $2 \times 10^{-2}m$ on the window and $5 \times 10^{-2}m$ on the truck front surfaces. The element sizes of the trimmed mesh are $5 \times 10^{-2}m$ on the interfaces of the partition block. The maximum size of the trimmed elements is $0.5m$.

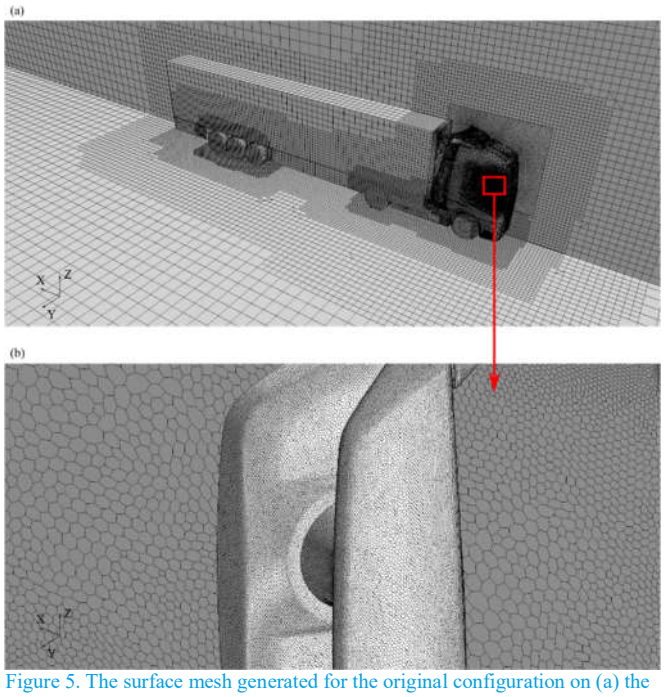

Figure 5. The surface mesh generated for the original configuration on (a) the entire geometry (b) the window and upper mirror head. The red rectangle in subfigure (a) marks the region that is magnified in subfigure (b).

The study of mesh independence is performed based on the simplified geometry. Three meshes with different levels of the refinement are used. The information of the meshes are listed in Table 1. The minimum and maximum lengths of the elements are denoted by Δ_{min} and Δ_{max}. The wall-normal heights of the elements nearest the walls are represented by Δh_1. The time-averaged values and the spectra of the pressure and velocity fluctuations at the monitors on the window and in the wake from the mirror have been compared between the meshes. For the sake of brevity, the figures plotted for the comparison are not presented here. These quantities obtained from the different meshes are consistent. Hence, the coarsest mesh (Case 1) is sufficient to resolve the flow. It is employed in the subsequent analysis.

Table 1. The information of the meshes for the simplified geometry.

Case No.	$\Delta_{min}\ (m)$	$\Delta_{max}\ (m)$	Δh_1 (m)	Total Number of Nodes
1	5×10^{-3}	0.5	4×10^{-5}	4.1×10^{7}
2	2.5×10^{-3}	0.25	4×10^{-5}	6.7×10^{7}
3	1.5×10^{-3}	0.2	2×10^{-5}	1.63×10^{8}

Since the same mirror and A-pillar are assembled in the simplified and original geometries, it is believed that the range of length scales of the turbulence in the wakes from these components will be similar between the geometries. The same mesh parameters are taken to

generate the mesh for the original geometry, which is also described in Figure 5.

6. Results and Discussion

The time-averaged drag coefficient is defined as $C_D = D/(0.5\rho_\infty U_\infty^2 A_{ref})$, where D denotes the time-averaged drag, U_∞ is the freestream streamwise velocity, ρ_∞ denotes the freestream density, and A_{ref} is the reference area. Table 2 gives C_D of the mirror based on $\rho_\infty = 1.17\ kg/m^3$ and $A_{ref} = 1m^2$. The difference between the coefficients of the geometries is small. The simplified geometry is thus suitable to predict the time-averaged drag for the mirror.

Table 2. The time-averaged drag coefficient of the mirror.

	Original geometry	Simplified geometry
C_D	0.854	0.855

Defining the time-averaged pressure as $\bar{p} = \langle p - p_\infty \rangle$, its magnitudes on the window are compared between the original and simplified geometries in Figure 6. Consistent results between the geometries are observed. Therefore, the present simplifications are valid for the prediction of the mean pressure. A low-pressure region is found near the A-pillar. This region is formed due to the flow separation at the A-pillar. The separation causes the turbulent structures and mean reattachment occurring in the region of strong surface-pressure gradients, which is indicated by the quick transition of the pressure contours from blue to yellow. This behavior will be further demonstrated in the subsequent analysis in terms of streamlines and resolved turbulence kinetic energy (TKE).

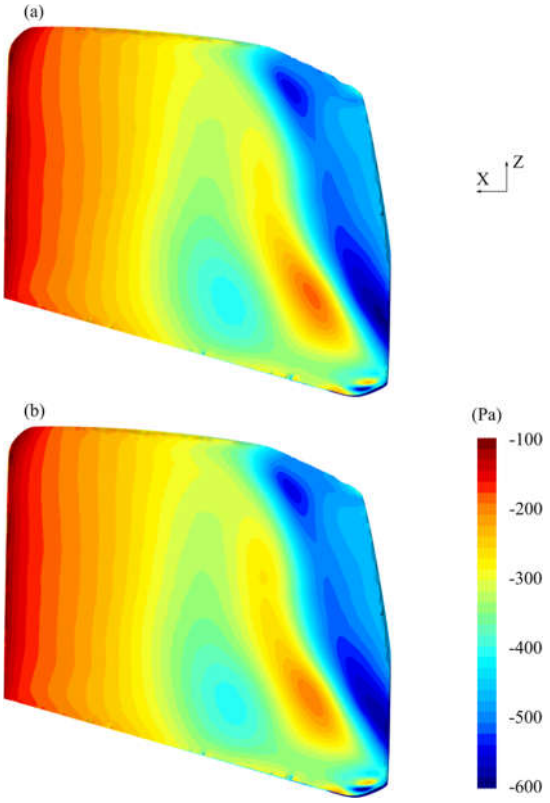

Figure 6. The time-averaged pressure on the window: (a) the original geometry and (b) the simplified truck geometry.

The flow quantities of the original and simplified truck geometries are compared at predefined monitors. The monitor positions are shown in Figure 7. The monitors named M1 and M2 are positioned on the window surface downstream of the upper and bottom mirror heads, respectively. The monitors, M3 and M4, are located in the wakes induced by the mirror heads.

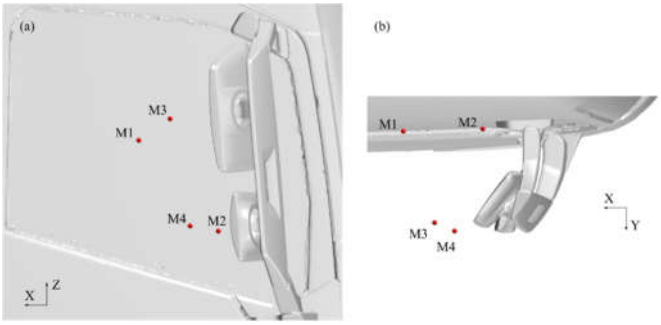

Figure 7. The positions of the monitors. M1 and M2 are located at the window surface.

The power spectral densities (PSDs) of the pressure fluctuations at M1 and M2 are displayed in Figure 8. The magnitudes obtained from the simplified geometry agree with those from the original geometry. This indicates that the simplified geometry can reproduce the characteristics of the surface pressure fluctuations on the window, which come from the impingement of the flow structures induced by the side-view mirror and A-pillar. Furthermore, energy peaks are observed at 645 Hz and 1147 Hz. The peaks are associated with the characteristic frequencies of the shear layers developing from the mirror edges.

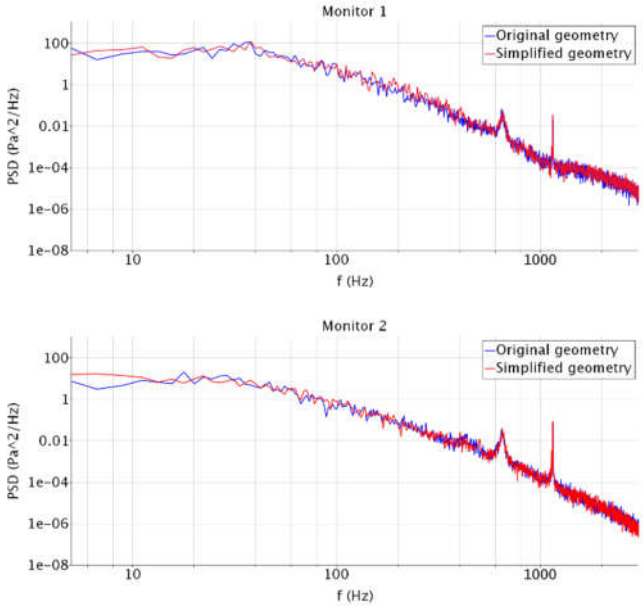

Figure 8. The PSDs of the pressure fluctuations at the monitors M1 and M2.

The PSDs of the pressure fluctuations as a function of frequencies are displayed for M3 and M4 in Figure 9. The results between the original and simplified geometries are consistent. This consistence indicates that the simplifications can retain the characteristics of the wakes induced by the upper and bottom mirror heads. In addition, there are no significant peaks in the spectra. This feature is different from the surface pressure fluctuations shown in Figure 8.

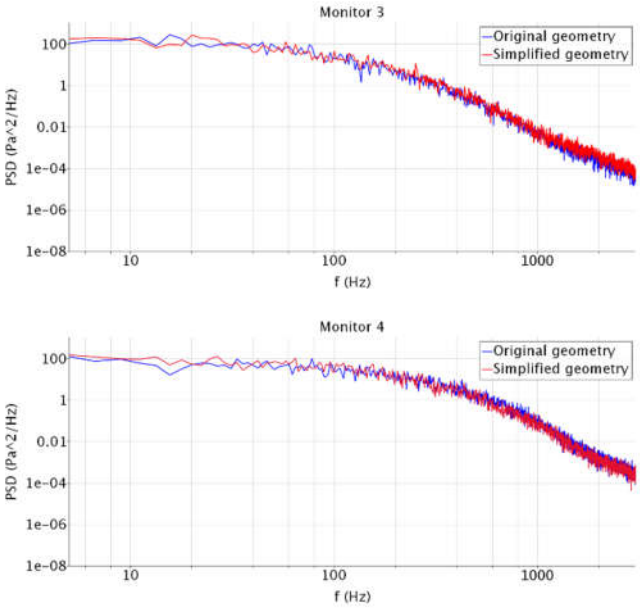

Figure 9. The PSDs of the pressure fluctuations at the monitors M3 and M4.

The PSDs of the streamwise velocity fluctuations at M3 and M4 are shown in Figure 10. Consistent results are observed for the geometries. The other velocity components also have the same behaviors. They are not presented for the sake of brevity. The observation suggests that the simplifications have negligible influence on the statistics of the velocity fluctuations in the wakes that are induced by the mirror heads.

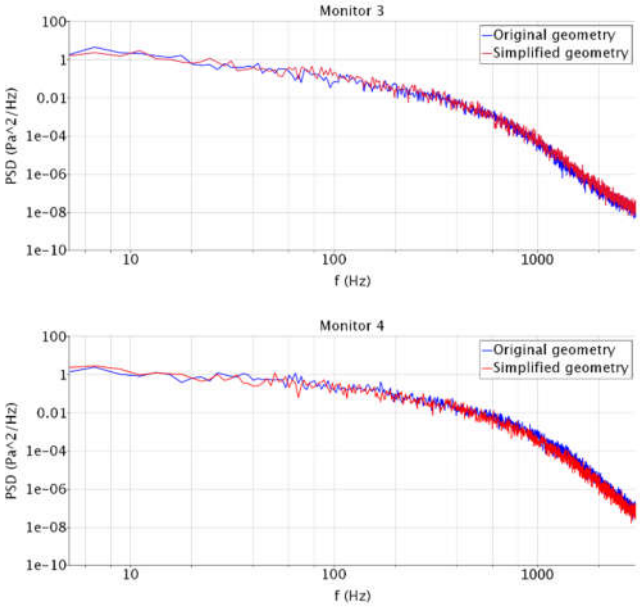

Figure 10. The PSDs of the streamwise velocity at the monitors M3 and M4.

To identify the flow structures downstream of the mirror, a snapshot of isosurfaces of the vorticity magnitude at $2 \times 10^3\ s^{-1}$ for the simplified truck geometry is illustrated in Figure 11. Many vortices are seen behind the mirror. This indicates that the mirror plays an important role in the generation of the noise sources near the window [13]. The important role of the mirror in the production of the turbulence and noise is also commonly reported for cars [14].

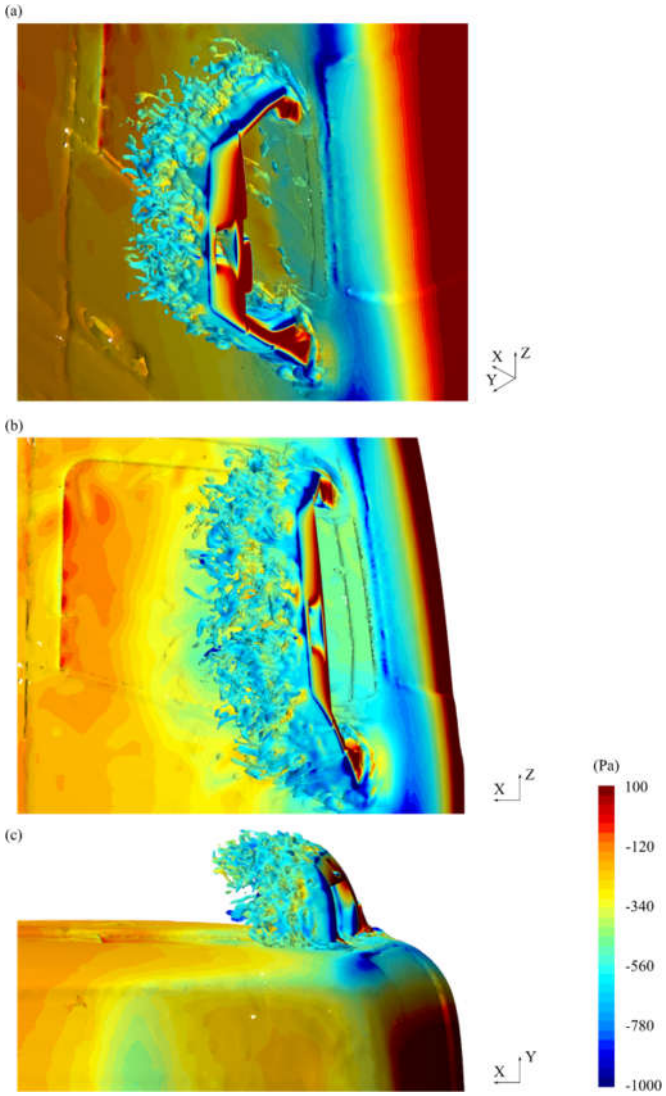

Figure 11. A snapshot for isosurfaces of the vorticity magnitude at $2 \times 10^3\ s^{-1}$ produced by the simplified truck geometry. The isosurfaces are colored with the contours of the instantaneous pressure, for which p_∞ has been subtracted.

The flow structures produced by the simplified truck geometry are further identified based on the Q-criterion at 1×10^5 in Figure 12. The A-pillar also induces vortices under the mirror although the amount of the vortices is lower than for the mirror. Note that these vortices cannot be discerned based on the vorticity magnitudes. The reason is that the strength of the vortices from the A-pillar is lower than those from the mirror. Moreover, the window is subjected to the impingement of the vortices from the A-pillar. The impingement can exert fluctuating hydrodynamic pressure on the window.

Streamlines for the time-averaged velocity of the simplified geometry are shown in Figure 13. The flow separation at the A-pillar is indicated. The streamlines from the A-pillar reattach to the window in the region of high pressure gradients. No reattachment is observed for the streamlines from the mirror. The A-pillar is thus important to produce the hydrodynamic impingement that is associated with the reattachment.

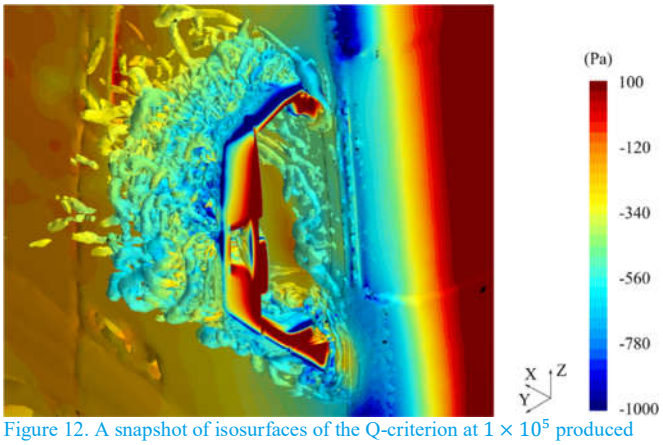

Figure 12. A snapshot of isosurfaces of the Q-criterion at 1×10^5 produced by the simplified truck geometry. The isosurfaces are colored with the contours of the instantaneous pressure, for which p_∞ is subtracted.

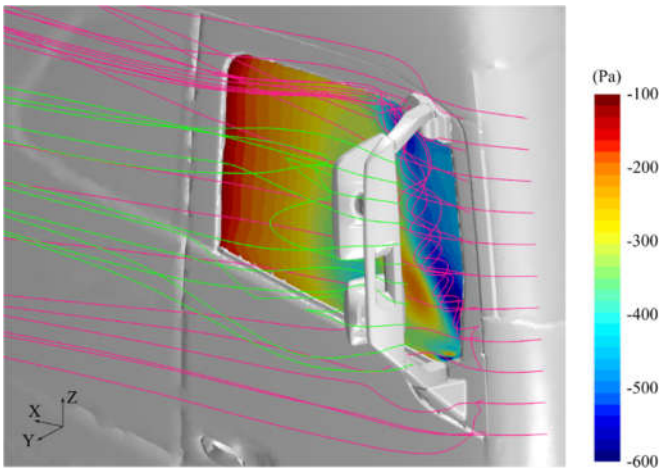

Figure 13. Streamlines for the time-averaged velocity (those from the A-pillar in purple and those from the mirror in green) and contours of the time-averaged surface pressure on the window, drawn for the simplified geometry.

The resolved TKE in the wakes of the mirror heads, compared to the root mean square values (RMS) values of the pressure fluctuations on the window, is shown in Figure 14. The high TKE near the window is caused by the shear layers developing from the inner side-edges of the mirror heads that are close to the window. Moreover, the high TKE is caused by the turbulent flow due to the flow separation at the A-pillar. The distribution of large RMS values of the pressure fluctuations follows the regions of the high TKE. The reason is that the impingement of the turbulence induced by the inner side-edges and A-pillar produces significant hydrodynamic pressure fluctuations.

The RMS values of the pressure fluctuations on the window are also illustrated in Figure 15. It is observed that the results between the two geometries are consistent. The regions of high energy are identified. Regions 1 and 2 are caused by the upper and bottom mirror heads, respectively, as indicated in Figure 14. Region 3 results from the A-pillar. The energy levels of Region 3 are higher than the other regions. The reason is that the vortices from A-pillar exert direct and strong impingement (see Figures 12 and 14) although their strengths are weaker than the shear layers (see Figures 11 and 14). In addition, a small region of very high energy is observed near the bottom corner. The shear layer initiating from the bottom part of the mirror bracket is the cause of this region.

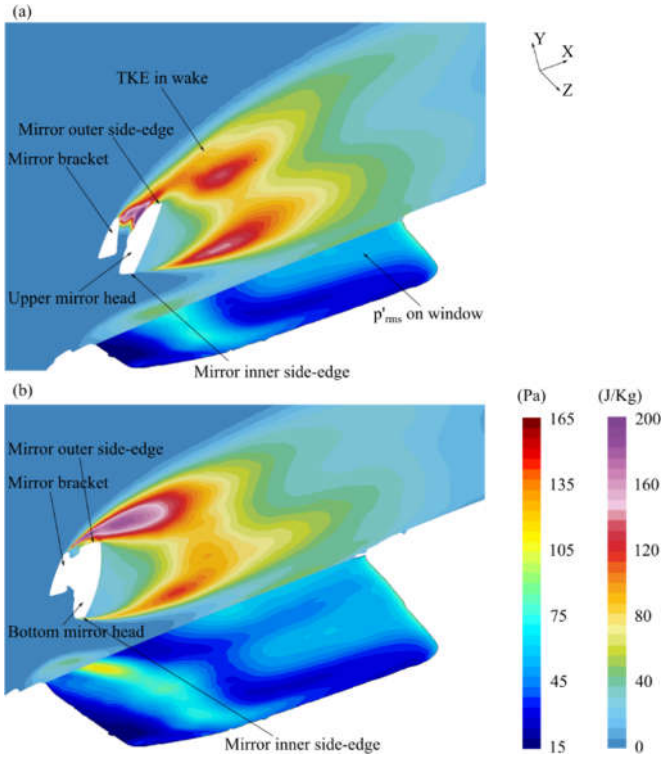

Figure 14. The resolved TKE in the planes (a) near the middle of the upper mirror head and (b) in the middle of the bottom mirror head, as well as the RMS values of the surface pressure fluctuations on the window, drawn for the simplified geometry.

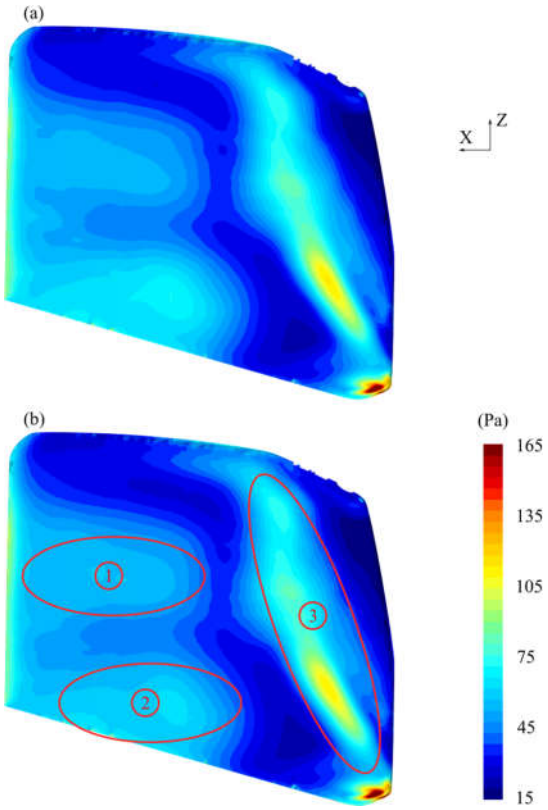

Figure 15. The RMS values of pressure fluctuations on the window: (a) the original geometry and (b) the simplified truck geometry, where the high-energy regions are marked with red lines.

To address the characteristic frequencies of the free shear layers, monitors are set near the side-edges of the mirror heads. The locations of the monitors are illustrated in Figure 16. The PSDs of the pressure fluctuations at the monitors are displayed in Figure 17. The results are compared with the surface pressure fluctuations at M2 on the window. No peaks are seen at M5 and M7 in the shear layers from the outer side-edges. The reason is that the shear layer from the bracket upstream of the mirror impinges on the outer side-edges and triggers powerful turbulence (see Figure 14). In contrast, the effect of the bracket on the inner side-edges is not obvious. Peaks at 1147Hz are thus captured at M6 and M8, which are located in the shear layers developing from the inner side-edges. The same frequency is also found in the surface pressure fluctuations. This suggests that the fluctuations at this frequency are associated with the inner shear layers. Large magnitudes of a semi-broadband type are observed between 200Hz and 1000Hz without noticeable peaks at 645Hz, which is another peak frequency of the surface pressure fluctuations. The present results are therefore insufficient to demonstrate whether this peak frequency results from the inner shear layers. An extensive study to confirm the cause of this peak frequency is ongoing in the authors' group.

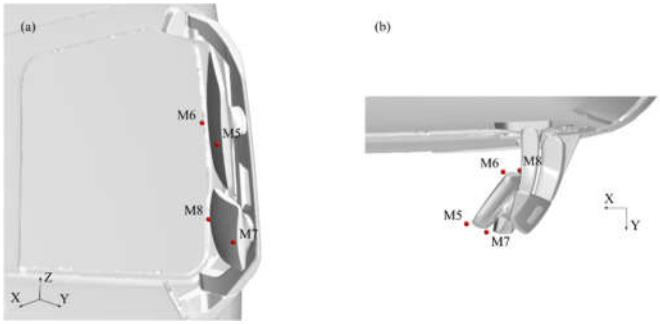

Figure 16. The locations of the monitors near the mirror edges.

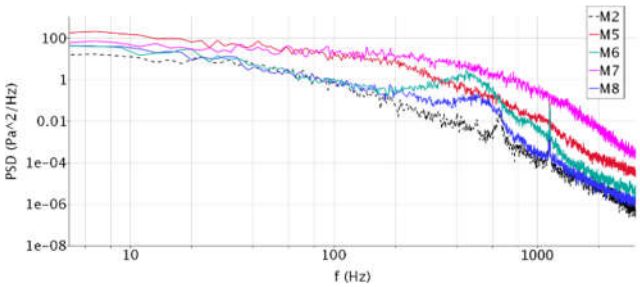

Figure 17. The PSDs of the pressure fluctuations computed for the simplified geometry. Note that M2 is located on the window, as shown in Figure 7.

7. Summary

The flow induced by a production side-view mirror mounted on a full-scale truck is simulated with compressible improved delayed detached eddy simulation (IDDES). A simple numerical strategy of investigating the installation effect for the mirror is presented. In this strategy, very coarse elements are generated for the mesh in the region that are far away from the mirror, whereas refined elements are constructed near the mirror and the region of the wakes induced by the mirror. The strategy leads to a RANS type computation in the region of the coarse elements and a LES type computation in the refined elements region. As the total number of elements is reduced by means of the usage of the coarse elements, the computational resources are saved.

The installation effect of the side-view mirror is investigated using the simple numerical strategy. Since the size of the full-scale truck geometry is large and the geometry is complex, a convenient way of simulating the installation effect is to well resolve the flow only near the mirror. Furthermore, some simplifications are applied to reduce the complexity of the original truck geometry. The total number of the mesh elements is decreased since the details of the geometry are removed by the simplifications and are not resolved in the mesh. In the simplified geometry, the small-scale gaps at the connections between the surfaces are sealed. The truck front and the trailer are connected so that the large gap between them is removed. The trailer body is modified to an apex-truncated square pyramid. The wheels under the trailer are eliminated. Half of the configuration is simulated with the application of the symmetry boundary condition.

The results of the original and simplified geometries are compared in terms of the surface pressure on the window, the surface pressure fluctuations, and the pressure and velocity fluctuations in the wakes behind the mirror. It is found that the simplified geometry reproduces the flow field surrounding the mirror. Furthermore, the surface pressure fluctuations are found with peaks at 1147 Hz. The peaks are related to the free shear layers that initiate from the inner side-edges of the mirror heads. The present approach is suitable specifically for the evaluation of the turbulent flow surrounding the mirror region. It is assumed to be applicable for the aeroacoustics evaluation, but such evaluation is not performed in the present study and thus will be an interesting future work.

References

1. George, A. R., "Automobile Aerodynamic Noise," SAE Technical Paper 900315, 1990.
2. Ask, J., and Davidson, L., "The Sub-Critical Flow Past a Generic Side Mirror and Its Impact on Sound Generation and Propagation," AIAA Paper 2006-2558, 2006.
3. Saltzman, E. J., and Meyer, R. R. Jr., "A Reassessment of Heavy-Duty Truck Aerodynamic Design Features and Priorities," NASA/TP-1999-206574, 1999.
4. Spalart, P.R., Jou., W.H., Strelets, M., and Allmaras, S.R., "Comments on the Feasibility of LES for Wings, and on a Hybrid RANS/LES Approach," 1st AFOSR Int. Conf. on DNS/LES Aug, 4-8 1997. In: Advances in DNS/LES, C. Liu and Z. Liu Eds., Greyden Press, Columbus, OH.
5. STAR-CCM+ User Guide (Version 12.04), Siemens PLM Software, 2017.
6. Yao, H.-D., Chroneer, Z., and Davidson, L., "Investigation of Interior Noise from Generic Side-View Mirror Using Incompressible and Compressible Solvers of DES and LES", SAE Technical paper, 2017.
7. Shur, M.L., Spalart, P.R., Strelets, M.Kh., and Travin, A.K., "A Hybrid RANS-LES Approach with Delayed-DES and Wall-Modelled LES Capabilities," International J. Heat and Fluid Flow, 29(6):1638-1649, 2008.
8. Wilcox, D.C., "Turbulence Modeling for CFD, 2n Edition," (DCW Industries Inc., 1998).
9. Colonius, T., Lele, S. K., and Moin, P., "Boundary Conditions for Direct Computation of Aerodynamic Sound Generation." AIAA J. 31:1574-1582, 1993.
10. Yao, H.-D., Davidson, L., and Eriksson, L.-E., et al., "Surface Integral Analogy Approaches to Computing Noise Generated by a 3D High-Lift Wing Configuration," AIAA paper, 2012-0386.
11. Yao, H.-D., Davidson, L., and Eriksson, L.-E., et al., "Surface Integral Analogy Approaches for Predicting Noise from 3D

High-Lift Low-Noise Wings," Acta Mech. Sin. 30(3):326-338, 2014.
12. Yao, H.-D., Davidson, L., and Eriksson, L.-E., "Noise Radiated by Low-Reynolds Number Flows past a Hemisphere at Ma=0.3," Phys. Fluids 29(7):076102, 2017.
13. Williams, J. E. F., Hawkings, D. L., "Sound Generation by Turbulence and Surfaces in Arbitrary Motion". Philos. Trans. R. Soc. A 264(1151): 321-342, 1969.
14. Becker, S., Nusser, K., and Oswald, M., "Aero-Vibro-Acoustic Wind Noise-Simulation Based on the Flow around a Car," SAE Technical Paper 2016-01-1804, 2016.

Contact Information

Mailing address: Department of Mechanics and Maritime Sciences, Chalmers University of Technology, Horsalsvagen 7A, Gothenburg, Sweden, SE-41296

Email address: huadong.yao@chalmers.se

Telephone number: +46 31 772 1405

Acknowledgments

This work has been supported by Fordonsstrategisk Forskning och Innovation (FFI) of VINNOVA-Sweden's innovation agency (grant no. 2014-01386). The authors offer their appreciation to the Swedish National Infrastructure for Computing (SNIC), who provided computer resources.

Definitions/Abbreviations

LES	large eddy simulation
DES	detached eddy simulation
IDDES	improved delayed DES
RANS	the Reynolds-averaged Navier–Stokes equations